PAPER

Check for updates

Synthesis, structure and spectroscopic properties of BODIPY dyes incorporating the pentafluorosulfanylphenyl group†

Richard D. James, Fabio Cucinotta, [ID] Paul G. Waddell and
Andrew C. Benniston [ID] *

Six compounds (**BD1–BD6**) are discussed based on the borondipyrromethene (BODIPY) core and functionalised in the *meso* position or the 3,5-positions with pentafluorosulfanylaryl subunits. The SF$_5$ unit in the aryl ring acts an electron-withdrawing group and its effect on the properties of the BODIPY derivatives is described. Two crystal structures were obtained for the simplest compounds in which the *meso* position of the BODIPY is either pentafluorosulfanylphenyl (**BD1**) or pentafluorosulfanylphenylethynylphenyl (**BD2**). The crystal packing features of the two structures were used to rationalise the strong solid-state emission observed for the two compounds in terms of exciton-coupled dimers. Solution phase photophysical properties of the compounds are also described, and trends within them are discussed in terms of the negative hyperconjugation and the "non-bonded" resonance effect of the SF$_5$ group. The long-wavelength absorbing and fluorescing dyes (**BD4–BD6**) are π-conjugated at the 3,5 positions, but they do not display typical solvatochromic behaviour associated with push–pull chromophores. The alterations in their absorbance and fluorescence maxima with change in solvent are adequately fitted to the solvent polarizability function ($f(n^2) = (n^2 - 1)/(2n^2 + 1)$), where n is the refractive index. The good linear fit supports no major change in the electronic transition dipole moment between the ground and excited states. Density functional theory (DFT) calculations were consistent with localised low-energy π–π* transitions rather than any charge-transfer transitions despite the existence of the electron-withdrawing SF$_5$ group(s).

Introduction

Since its initial discovery over some fifty years ago, the boron dipyrromethene (BODIPY) group has grown in stature to a point where it is the choice dye for numerous chemical and biophysical applications.[1] The popularity of the dye can be attributed to several factors, arising not only from its highly beneficial photophysical properties (*e.g.*, high fluorescence quantum yield), but also to the ease at which it can be functionalised with disparate groups and in multiple positions of the chromophore backbone.[2] This versatility has given rise to a library of compounds, tuneable in both their colour and fluorescence signal output.[3] In this context, our own work focussed on the "fluorine effect" by incorporation of a fluoroaryl subunit, with different numbers and substituent patterns of fluorines, in the

meso position.[4] The highly electron-withdrawing nature of the fluoroaryl group afforded strongly fluorescent BODIPY dyes with tuneable redox properties. As a continuation to this work, the highly electron-withdrawing (pentafluorosulfanyl)phenyl (PFSP) unit was targeted, since it has found application in several push–pull structures that display solvatochromic properties.[5] The group is also of special interest because of its ability to participate in negative hyperconjugation. To assess the effect of the PFSP group on the BODIPY chromophore, two sets of compounds were pursued based on substitution at the *meso* site and the 3,5 positions. The examples were developed as highly conjugated systems, in addition bearing a protected carboxylic acid as a masked site for future semiconductor attachment (Scheme 1).
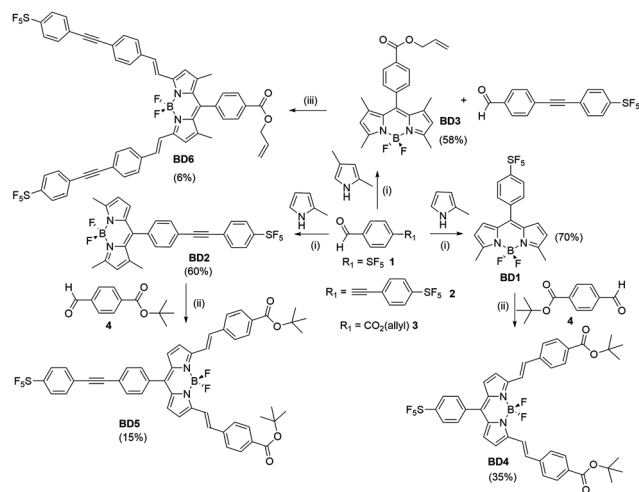
Results and discussion

Synthesis and characterization

The target compounds were prepared using standard methods starting from the commercially available compound **1**, or the derivative **3** synthesised using a literature procedure.[6]

Chemistry-School of Natural & Environmental Sciences, Newcastle University,
Newcastle upon Tyne, NE1 7RU, UK. E-mail: andrew.benniston@newcastle.ac.uk
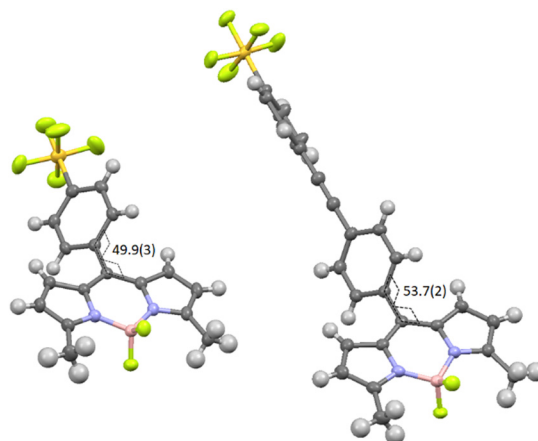
Scheme 1 Reagents and Conditions: (i) DCM, TFA, DIPEA, *p*-chloroanil or DDQ, BF₃·Et₂O, r.t. (ii) Piperidine, AcOH, MeCN, 3 Å molecular sieves, r.t. (iii) Piperidine, TsOH, toluene, Dean-Stark. Percentage yield given in brackets.

Fig. 1 X-Ray determined molecular structures for **BD1** (left) and **BD2** (right) as thermal ellipsoids (50%). Torsional angle shown in degrees with error in brackets. Sulphur = yellow, fluorine = green, nitrogen = blue, boron = pink, carbon = dark grey and hydrogen = light grey.

The previously unpublished compound **2** was prepared in 94% yield by Sonogashira coupling of 1-bromo-4-pentafluorosul-fanylbenzene with 4-ethynylbenzaldehyde. The preparation of **BD1** and **BD4** was reported in a prior publication.[7] The condensation of an appropriate aldehyde (**2** or **3**) with either 2-methylpyrrole or 2,4-dimethylpyrrole, coupled with oxidation and chelation to a BF₂ unit, afforded the BODIPYs **BD2** and **BD3** in reasonable yields. These BODIPY compounds along with **BD1** were the basis for performing the classic Knoevenagel condensation reaction at the 3,5 methyl groups. The condensation reaction of **BD1** with the *t*Bu protected carboxylic acid **4** by simply using MeCN as solvent at room temperature, and driving the reaction using molecular sieves, is known to work well to produce **BD4** as a blue solid.[7] The Knoevenagel condensation of **BD2** with **3** under identical conditions was not successful and heating to 60 °C was required to produce **BD5**. The same could not be said for the reaction of **BD3** with **2** under room temperature conditions, or slight heating, as no product was isolated. The harsher condition of reflux in toluene using a Dean-Stark apparatus to remove the water did succeed, but the yield of the product **BD6** was very low. The two 3,5-methyl groups for **BD1**, and to a lesser extent in **BD2**, are likely activated to deprotonation by the presence of the electron-withdrawing PFSP unit in the *meso* position. All compounds were analysed by standard analytical techniques. A typical ¹⁹F NMR spectrum for a PFSP containing compound displayed the expected splitting patterns, in addition to the quartet for the BF₂ unit, a doublet (equatorial F) and quintet (axial F) for the SF₅ group (see ESI† Fig. S25).
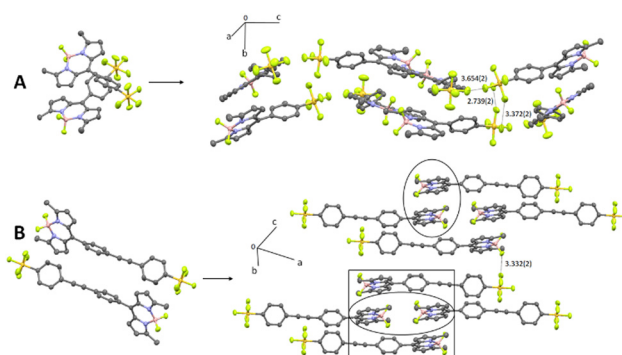
Further confirmation of the structures of **BD1** and **BD2** was obtained by single-crystal X-ray crystallography (Fig. 1). The basic dipyrromethene subunit for both structures is essentially identical with bond lengths and angles consistent with previously published structures.[8] The first subtle modification in the structures is observed at the dihedral angle relating to the

twist of the directly linked *meso* aryl group. This angle is slightly greater for **BD2** (53.7(2)°) when compared to **BD1** (49.9(3)°). The small variation is attributed to packing effects, since the crystal packing diagrams for the two compounds are vastly different (see later). The bond lengths and angles for the SF₅ are within error the same for both structures. The extra ethynylaryl spacer for **BD2** results in a linearly extended structure noting that the two aryl rings are non co-planar.

The most significant difference between the two structures relates to their respective packing diagrams and the way the two BODIPY subunits align (Fig. 2). A pair of **BD1** molecules arrange almost anti-parallel in a cross-like motif which extends in one dimension to give the impression of a wave modulating within the crystal. The SF₅ groups of disparate **BD1** units are prearranged such that specific F–F intermolecular distances fall within the range 3.7–3.4 Å. In comparison, an offset head-to-tail motif is observed for a pair of **BD2** molecules in the unit cell, which gives rise to a crystal packing diagram that can be highlighted as pseudo-dimers and -tetramers of BODIPY moieties. The packing features for both the BODIPYs are

Fig. 2 Crystal packing diagrams for **BD1** (A) and **BD2** (B) based on their simple dimers. Hydrogens are omitted for clarity and distances are given in Ångstroms. The circle highlights a pseudo-dimer and the square a pseudo-tetramer of BODIPYs.

considered important in the context of crystal emission as described later.

DFT calculations

The energy and spatial location of frontier molecular orbitals for BODIPY derivatives have been used extensively to rationalise their ground- and excited-state properties. Density functional theory (DFT) is commonly applied alongside its time-dependent analogue (TD-DFT) to identify electronic transitions.[9] Both these methods, and by employing the B3LYP functional and the 6-311G(d,p) basis set, were applied to the energy-minimised structures of **BD1–BD6** *in vacuo*. For comparison purposes, the calculated frontier molecular orbitals of **BD1** and **BD2** are illustrated in Fig. 3. The HOMOs for both compounds are located on the dipyrromethene backbone and are similar in appearance with a node located at the *meso* position as observed for other simple BODIPY derivatives. The energy difference ($\Delta = E_{HOMO}^{BD1} - E_{HOMO}^{BD2}$) is −0.14 eV. The LUMOs for **BD1** and **BD2** are again similar in appearance despite the presence of the additional ethynylaryl group. The energy difference ($\Delta = E_{LUMO}^{BD1} - E_{LUMO}^{BD2}$) is −0.068 eV. Whereas the LUMO+1 for **BD1** is exclusively located on the SF$_5$ group, the LUMO+1 for **BD2** is very much situated on the second aryl ring; this feature is more associated with the LUMO+2 for **BD1**. Even the LUMO+2 for **BD2** does not exhibit a feature consistent with electron density located on the SF$_5$ group. There is a distinct similarity of HOMO−1 for **BD1** with the HOMO−2 for **BD2**; their difference in energy is 1.79 eV. The HOMO−1 for **BD2** is clearly associated with the diarylethynyl subunit. The calculations predict that any electron addition/removal for both compounds will be essentially focussed at the dipyrromethene core. Only for **BD1** could electron addition be anticipated to occur at the SF$_5$ unit.

The application of TD-DFT to the two compounds identified the first three main electronic transitions, their associated orbital contributions and energies (Table 1). The first point to note is the similarity in the energy for the first electronic transition and orbital contribution when comparing **BD1** with **BD2**. Even though there is a small involvement of a HOMO−2 to LUMO electronic transition for **BD2**, all the orbitals in both cases are located on the dipyrromethene core consistent with a π–π* absorption. The ratio of oscillator strengths corresponding to **BD1**/**BD2** is 1.34, indicating a slightly more favourable electronic transition for the smaller BODIPY. In contrast, the oscillator strength for the second electronic transition (HOMO−1 to LUMO) of **BD1** is calculated to be some six times smaller than the corresponding one for **BD2**. This difference is explained by the alteration in the molecular orbital shape for the HOMO−1 in **BD2** (Fig. 3), which is extended onto the *meso* diarylethynyl subunit. In fact, the electronic transition would appear to shift electron density from the *meso* substituent onto the dipyrromethene group more reminiscent of charge-transfer. This charge-transfer character is also observed in the third electronic transition for **BD2**, along with electron migration from the dipyrromethene unit to the diarylethynyl subunit. A weak third transition with some charge-transfer character is also calculated for **BD1**.

Similar calculations to above were performed on the carboxylic acid derivatives for the remaining BODIPY examples and the results are collected in ESI† (Fig S1–S4). The main point to note is the predicted ordering for the energies of the first electronic transition **BD5** (2.23 eV) > **BD4** (2.12 eV) > **BD6** (2.07 eV), corresponding to the BODIPYs with further π-conjugation at the 3,5 positions.

Electrochemistry

Cyclic voltammetry (CV) and square-wave voltammetry (SWV) techniques were used to assess the redox properties of the BODIPY compounds in acetonitrile, probing more directly the HOMO and LUMO orbital energies and assessing any substituent effects. The redox behaviour for **BD1** is highlighted as an example, and collected in Table 2 are selected oxidation and reduction potentials for the other compounds. The CV and SWV recorded for **BD1** in acetonitrile containing 0.2 M tetrabutylammonium hexafluorophosphate (TBAHFP) *versus* ferrocene reference are shown in Fig. 4. The oxidative segment of the CV displayed a clear irreversible one-electron wave at +0.89 V (*vs.* FcH) corresponding to formation of the radical cation. The lack of the reverse wave is consistent with the partially substituted dipyrromethene core and deprotonation of the radical cation. The SWV indicates there are at least two more oxidations. The reductive segment of the CV exhibits a quasi-reversible one-electron wave at −1.26 V (*vs.* FcH). Upon further scanning to a more negative potential an irreversible wave is observed at −2.04 V (*vs.* FcH); a partial wave corresponding to oxidation of the initially generated dianion is observed at −1.47 V (*vs.* FcH). The significant difference between the two waves supports a significant chemical/structural transformation of the dianion initially formed. The irreversible wave is likely a mixture of two one-electron reductions of the initially formed dipyrromethene-based radical anion and the PFSP group.

The electrochemistry response for the remaining derivatives **BD2–BD6** was also recorded, and for simplicity only the first oxidation and reduction potentials are highlighted (Table 2). Several points are worth emphasising when comparing the redox values across the series. The greater π-expanded compounds **BD4–BD6** are the easiest to reduce; the hardest to
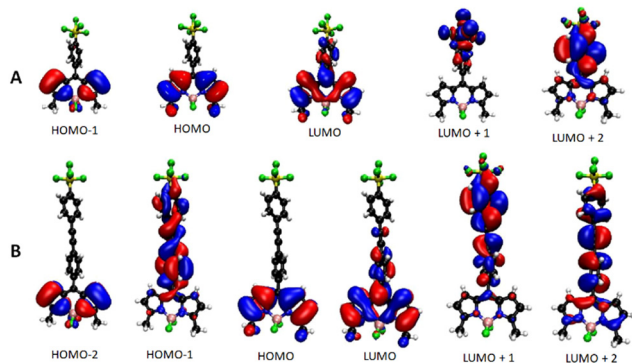

Fig. 3 DFT calculated Kohn–Sham molecular orbitals using the B3LYP functional and the 6-311G(d,p) basis set for **BD1** (A) and **BD2** (B).
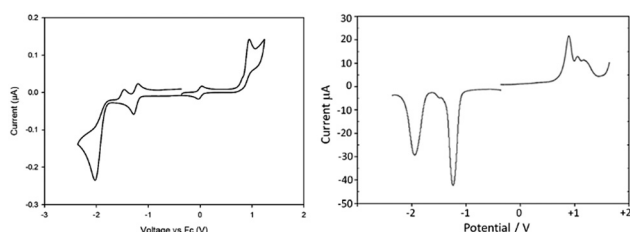
Table 1 TD-DFT calculated electronic transitions for compound **BD1** and **BD2** *in vacuo*

Cmp	Electronic transition (oscillator strength)	Orbitals (% contribution)	Energy/eV (nm)
BD1	1 (0.4867)	HOMO → LUMO (100)	2.94 (422)
	2 (0.0579)	HOMO−1 → LUMO (98) HOMO → LUMO (2)	4.02 (308)
	3 (0.0146)	HOMO → LUMO+2 (100)	4.55 (273)
BD2	1 (0.3627)	HOMO → LUMO (94)	2.97 (417)
		HOMO−2 → LUMO (6)	
	2 (0.3774)	HOMO−1 → LUMO (100)	3.44 (360)
	3 (0.0014)	HOMO−2 → LUMO (49)	3.53 (351)
		HOMO → LUMO+1 (46)	
		HOMO → LUMO+2 (4)	

Table 2 Electrochemistry data recorded for a series of BODIPY compounds in CH_3CN using cyclic voltammetry. Potential *vs.* ferrocene as the reference
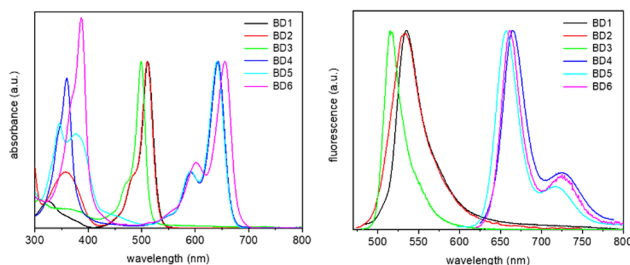
	BD1	BD2	BD3	BD4	BD5	BD6
E_{ox}/V^a	+0.89	+0.67	+0.82	+0.68	+0.89	+0.49
E_{red}/V^b	−1.26	−1.28	−1.58	−0.97	−1.03	−1.07
Δ/V^c	2.15	1.95	2.40	1.65	1.92	1.56

^{a} Irreversible wave. ^{b} $E_{1/2}$ value. ^{c} Difference between oxidation and reduction potentials.

Fig. 4 Cyclic voltammogram (left) and square-wave voltammogram (right) recorded for **BD1** in N_2-purged acetonitrile solution containing 0.2 M tetrabutylammonium hexafluorophosphate background electrolyte at a glassy carbon working electron. Scan rate = 100 mV s^{-1}. Note: the reversible wave at 0 V is the ferrocene FcH/FcH$^+$ couple.

reduce compound is **BD3** as expected because of the presence of the four electron donating methyl groups. The easiest compound to oxidise is **BD6** and coupled to its low reduction potential means that the energy gap Δ is the smallest. This energy difference ordering is **BD3** > **BD1** > **BD2** > **BD5** > **BD4** > **BD6**. Such prioritisation is relevant when considering the absorption properties of the compounds.

Fig. 5 Normalised absorption (left) and fluorescence (right) spectra, recorded for the six dyes in acetonitrile.

Photophysical properties

Electronic absorption and fluorescence spectra were recorded for **BD1**–**BD6** in dilute acetonitrile at room temperature. The normalized spectra are shown in Fig. 5 (see also ESI,† Fig. S5–S10) and collected in Table 3 are data for the series. The first point of note is the similarity of the absorption (λ_{ABS}) and fluorescence (λ_{EM}) maxima for **BD1** and **BD2**, despite their obvious structural differences. The similarity of the λ_{ABS} values was predicted by the DFT calculations, although the absolute numbers were *ca.* 90 nm too blue shifted. However, it is noted that the DFT calculated ratio for the oscillator strengths corresponding to **BD1/BD2** (1.34) is in good agreement with the observed ratio of 1.22 for the molar absorption coefficients (ε_{MAX}). The most noteworthy observation is the dramatic 4-fold drop in fluorescence quantum yield when comparing **BD2** to **BD1**.

To try and rationalise the result, the comparison of **BD1** with the phenyl (R = H) and cyanobenzene (R = CN) derivatives (Fig. 6A) is made.[10] The fluorescence quantum yield for **BD1** is more on par with the phenyl derivative, but the λ_{ABS} and λ_{FLU} values are comparable to the cyanobenzene compound; more significantly, the ϕ_{FLU} for **BD1** is 10-fold greater than this derivative. The Hammett coefficient for cyanide ($\sigma = +0.66$)[11] is remarkably similar to SF$_5$ ($\sigma = +0.68$),[12] so a simple electronegativity argument for the change is not convincing. The SF$_5$ group in the *para* position would appear to enhance the radiative rate constant (k_{RAD}) and reduce the non-radiative rate constant (k_{NR}). The concept of negative hyperconjugation of the SF$_5$ group is used to discuss its effect on push–pull fluorescent compounds.[13] The effect arises because of the sufficiently large

Table 3 Comparison of recorded and calculated photophysical parameters for the BODIPY derivatives in MeCN

Compound/Data	BD1	BD2	BD3	BD4	BD5	BD6
λ_{ABS} nm	511	511	499	642	641	655
λ_{EM} nm	535	535	516	665	657	669
ε_{MAX} M^{-1} cm^{-1}	69 500	57 000	55 000	79 500	43 000	30 000
SS^a cm^{-1}	878	878	660	539	380	320
ϕ_{FLU}^b	0.30	0.07	0.63	0.57	0.66	0.25
τ_s ps^c	487	296	2100	4970	4850	2130
k_{RAD} 10^8 s$^{-1 d}$	6.2	2.4	3.0	1.1	1.4	1.2
k_{NR} 10^9 s$^{-1 e}$	1.4	3.1	0.18	0.09	0.07	0.35

^{a} Stokes' shift. ^{b} Quantum yield of fluorescence. ^{c} First-excited singlet lifetime. ^{d} Radiative rate constant. ^{e} Non-radiative rate constant.

R = H, λ_{ABS} = 507 nm, λ_{EM} = 521 nm, ϕ_{FLU} = 0.17
R = CN, λ_{ABS} = 512 nm, λ_{EM} = 537 nm, ϕ_{FLU} = 0.030
Negative hyperconjugation   "no-bond" resonance

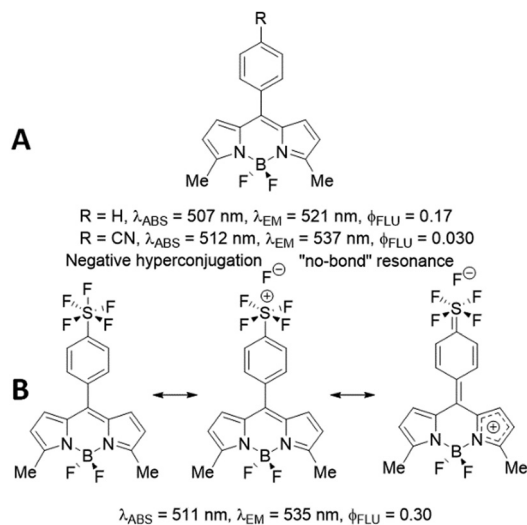λ_{ABS} = 511 nm, λ_{EM} = 535 nm, ϕ_{FLU} = 0.30

Fig. 6 Photophysical parameters for two literature reported BODIPYs (A) and the effect of negative hyperconjugation and "no-bond" resonance on **BD1** because of the SF$_5$ unit (B).

difference in electronegativity between sulphur and fluorine (valence-bond approach), or alternatively the overall calculated bond order of 3.84 (molecular orbital approach).[14] Evidently, the coupling of negative hyperconjugation and "no-bond" resonance (Fig. 6B) would result in enhanced double-bond character at the *meso*-aryl bond and consequently heightened rigidity in the structure. In the first-excited singlet state, this enriched rigidity would help reduce non-radiative processes. Of course, in the cyanobenzene BODIPY electron delocalization is also feasible, suggesting that the negative hyperconjugation coupled to "non-bonded" resonance has a stronger impact than simple resonance alone. The effect is "switched off" as the SF$_5$ is decoupled from the dipyrromethene core, as evidenced by the dramatic reduction in the ϕ_{FLU} for **BD2**.

The comparison of **BD4** with **BD5** is highlighted as they represent the π-extended versions of **BD1** and **BD2**, respectively. The absorption maxima, though shifted to the red as expected, for **BD4** and **BD5** are remarkably similar; a trend also observed for their smaller BODIPY counterparts. Their fluorescence maxima are different and separated by some 8 nm, which is in complete contrast to the trend seen for **BD1** and **BD2**. This difference is likely linked to the alteration of the orbitals associated with the electronic transitions, which for **BD4** and **BD5** are confined to the two aryl-ethene groups. There is not the same dramatic drop in fluorescence quantum yield comparing **BD4** with **BD5**, and values for ϕ_{FLU} are also reasonable for both compounds (∼60%). The SF$_5$ group and its proximity to the dipyrromethene core would appear to be much less important. The longest-wavelength absorbing dye is **BD6**, with an emission maximum close to that of **BD4**. As a consequence, the Stokes' shift is the smallest in the series, supporting a modest structural perturbation upon formation of the first-excited singlet state. Worth noting is the trend in λ_{ABS} in terms of energy is **BD3** > **BD1** = **BD2** > **BD5** > **BD4** > **BD6**, which is very similar to the trend observed in the difference between the oxidation and reduction potentials (Table 2).

Solvatochromic properties

The push–pull character of previously described donor–acceptor compounds incorporating the SF$_5$ unit displayed clear solvatochromic behaviour.[5] To ascertain if the same was applicable to **BD4**–**BD6**, absorption and fluorescence spectra were recorded in a range of solvents (see ESI† Fig. S11). Definite shifts in both λ_{ABS} and λ_{FLU} were observed. For each compound the difference ν_{ABS}–ν_{FLU} (in cm^{-1}) *versus* the solvent polarity function (Δf) was analysed in terms of the Lippert-Mataga equation (eqn (1)),[15] where ε is the dielectric constant and n is the refractive index.

$$\nu_{ABS} - \nu_{FLU} = \frac{2\Delta f}{hca^3}(\mu_{ES} - \mu_{GS})^2$$

where

$$\Delta f = \frac{\varepsilon - 1}{2\varepsilon + 1} - \frac{n^2 - 1}{2n^2 - 1}$$

The equation predicts a linear correlation which affords the difference in the dipole moment between the ground and excited state (μ_{ES}–μ_{GS}) within a spherical solvent cavity of radius "a". There was no discernible linear relationship for any of the compounds, suggesting that the dipole moment in their ground- and excited-states is similar (see ESI,† Fig. S13). The shifts observed for λ_{ABS} and λ_{FLU} are more adequately mapped to the solvent polarizability function $f(n^2) = (n^2 - 1)/(2n^2 + 1)$, which again matches with the concept that permanent dipoles, if they do exist, do not differ between the ground-state and the excited-state (see ESI† Fig. S12). It appears that there is no sign of any enhanced charge-transfer character in the first-excited singlet state because of the electron-withdrawing SF$_5$ group; this tenet is supported by the DFT calculations. It is also noted that strong fluorescence was observed for all the compounds despite the change in solvent polarity.

Solid state emission

Crystals of **BD1** and **BD2** glowed strongly red when exposed to a UV light source, and their fluorescence optical properties were measured (see Fig. 7 and ESI† Fig. S14 and S15). The emission spectrum of **BD1** displayed a clear peak centred at 603 nm which is some 68 nm red shifted with respect to the compound in fluid solution. A broad weaker tail is observed towards much longer wavelength, consistent with emission from a dimer. Excitation spectra collected by monitoring at several wavelengths were similar to one another, but very different to the absorption spectrum in solution. A clear peak is observed at 410 nm with two further broad peaks located at around 500 nm and 570 nm. The emission lifetime measured for the crystalline sample required fitting to three exponentials with lifetimes corresponding to 0.82 ns (31%), 3.2 ns (60%) and 9 ns (9%). The first component is at least comparable with the lifetime measured in solution, supporting that some fraction of the emission is likely from a monomer-like BODIPY, albeit with a non-radiative pathway that is less efficient when compared to the dye in fluid solution. The enhanced rigidity of the dye because of the constraint imposed by crystal packing would contribute to a reduction in the non-radiative rate constant.
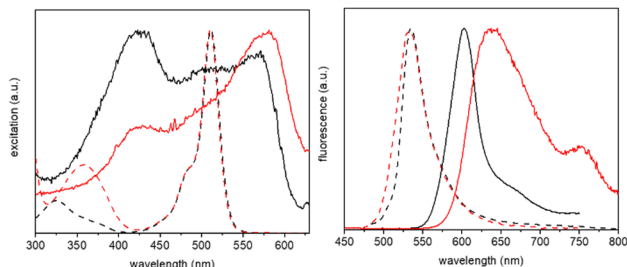
Fig. 7 Normalised excitation (left) and fluorescence (right) spectra of **BD1** (black, solid line) and **BD2** (red, solid line), recorded from crystalline samples, shown in comparison with the spectra from solution samples (dashed lines).

The emission spectrum for **BD2** was significantly more broadened compared to **BD1** with a clear maximum at 638 nm and a shoulder located at 750 nm. Again, the features are consistent with emission from a dimer, but the broadness is likely a result of multiple different sites as illustrated by the complexity of the packing diagram. The excitation spectrum in contrast to **BD1** showed a maximum at 579 nm, with a much smaller peak located at 425 nm. The emission lifetime measured for the crystalline sample required fitting to only two exponentials with lifetimes corresponding to 3.8 ns (48%) and 9.3 ns (52%). That no short lifetime component was required for the fit would suggest that monomer-like emission is not that significant.

The noticeably clear difference between the two compounds is evidently the result of their disparate crystal packing features as highlighted previously (see ESI† Fig. S16–S22). At a first level of interpretation, exciton coupling[16] of dimers would be anticipated to be quite different from inspection of the packing diagrams. For **BD1** there is a clear dimer which aligns the electronic transition dipoles at 86° with respect to each other, with a centre-to-centre distance of 5.1 Å. The exciton coupling in this dimer would be weak because of the near perpendicular arrangement of the two chromophores, explaining why some monomer-like emission is observed. A further two dimers are also discernible from the packing diagram, but in these cases the electronic transition dipoles are parallel or more co-linear, with centre-to-centre distances of 7.5 Å and 12.6 Å, respectively. In the classic exciton coupling model,[17] the parallel arrangement would result in a short-wavelength absorption band and the co-linear in a long-wavelength absorption band. This interpretation seems reasonable as both the features are observed in the excitation spectrum.

Two distinct dimers are observed for **BD2** within the crystal packing diagram, with centre-to-centre distances of 4.4 Å and 8.4 Å, respectively. The short-distance apart dimer represents an offset-stacked arrangement of dipyrromethene subunits. The second dimer places the dipyrromethene subunits in a head-to-head arrangement with parallel electronic transition dipoles. Two more dimer arrangements are observed between stacks in the packing diagram (viewed down *c*-axis), separated by 9.8 Å and 9.5 Å, respectively, with offset co-linear electronic transition dipoles (see ESI† Fig S21 and S22). The features observed in the excitation spectrum again can be explained by invoking a classic exciton coupling model.

Conclusions

The incorporation of pentafluorosulfanylaryl subunits into a BODIPY core is readily achieved at the *meso* or 3,5-positions, because of readily available starting materials or easily prepared precursors. Although the SF$_5$ unit within an aryl ring is electron withdrawing, its effect can be adequately discussed in terms of negative hyperconjugation and ''non-bonded'' resonance. In particular, direct linkage of the PFSP at the *meso* position of the dipyrromethene core appears to promote structural rigidity in the first-excited singlet state. As the group is decoupled from the dipyrromethene unit, its influence appears to diminish. This ''pentafluorosulfanyl effect'' may hold for other substitution patterns of BODIPY, or more significantly be universal to other chromophores. Hence, low fluorescence quantum yield flexible dyes may get an enhancement by its presence.

It is evident that the PFSP group is not an effectual electron acceptor, as evidenced in the electrochemistry findings and by the fact that no fluorescence quenching is observed even in highly polar solvents. Any charge-transfer state (CTS) associated with electron transfer from the BODIPY core to the PFSP group must be higher in energy than the emitting state; solvent stabilization is not strong enough to bring the CTS into play. In the solid state the situation is likely more complicated since the long lifetime of *ca.* 9 ns seen for **BD1** and **BD2** is unusual for J-like dimers. It is possible that a localised CTS associated with a dimer comes into play.

Experimental

Solvents for synthesis were used as received or dried by standard methods. Compounds were characterised by nuclear magnetic resonance (NMR) spectroscopy using Bruker Avance III 300 MHz, Bruker Avance III 400 MHz and Bruker Avance III HD 700 MHz spectrometers. Further analysis was performed using mass spectrometry (MS) and where possible by X-ray crystallography. UV-Vis spectroscopy measurements were conducted on a Shimadzu (UV-1800) UV/Vis spectrometer using 1 cm quartz cuvettes, 1 nm sample interval and ran in air unless otherwise stated. Emission and excitation measurements were run on a Shimadzu (RF-6000) fluorescence spectrometer using 1 cm quartz cuvettes and HPLC grade solvents where appropriate. Scan speed was 600 nm min^{-1} with slits at 3.0 nm for both source and detector unless otherwise stated. Quantum yield measurements were kept under 0.05 absorbance at the excitation wavelength to eliminate self-quenching and referenced *versus* either rhodamine 6G (λ_{em} = 480 nm, ϕ_{FLU} = 0.95 in methanol) or oxazine 1 (λ_{em} = 665 nm, ϕ_{FLU} = 0.11 in methanol).[18] Solid state and lifetime measurements were run using an Edinburgh FLS980 photoluminescence spectrometer, equipped with a 450 W Xenon arc lamp, Czerny Turner excitation and emission monochromators (1.8 nm mm^{-1} dispersion; 1800 grooves mm^{-1}), time-correlated single photon counting (TCSPC) module and a Hamamatsu R928 P photomultiplier tube (in a fan assisted TE cooled housing, operating temperature −20 °C). For lifetime measurements, samples were excited with an EPL-375 (370.8 nm; 61.1 ps pulse width) and an EPL-475 (471.8 nm;

61.1 ps pulse width) picosecond pulsed diode lasers and data analysis was performed on the F980 software with numerical data reconvolution based on Marquardt–Levenberg algorithm. Electrochemical characterisation used a three-electrode set-up with a platinum counter electrode, either a calomel or silver/ silver chloride reference electrode and a glassy carbon working electrode. The background electrolyte was a 0.2 M tetrabutylammonium hexafluorophosphate solution in dry acetonitrile which was degassed before each run. The setting used for DPV were a 0.2 V pulse for 0.02 seconds with a scan rate of 0.01 V s^{-1}. The setting used for square wave voltammetry are 0.01 V step with a 0.1 V amplitude at 20 Hz.

Computer calculations were performed using Gaussian 09[19] with Gauss view 5.0 to set up calculations and Visual Molecular Dynamics was used to render the images of the orbitals. All calculations where run on the University of Newcastle computing system Rocket HPC. The structures were either optimised before the energy calculations in vacuum or the structure was obtained *via* X-ray crystallography.

Preparation of 2

4-Ethynyl benzaldehyde (1.0 g, 7.7 mmol), [1,1′-bis(diphenylphosphino) ferrocene] dichloropalladium(II) (280 mg, 0.38 mmol), and copper(I) iodide (73 mg 0.38 mmol) were added to a 100 mL flame dried Schlenk flask under an inert nitrogen atmosphere. The flask was degassed three times. Toluene (30 mL) and diisopropylamine (5 mL) were added to a second flame dried Schlenk flask, the liquids were degassed using freeze pump thaw technique 5 times. The liquids were transferred to the first Schlenk flask *via* a cannula. The reaction was heated to 80 °C for 16 hours. The reaction was cooled to room temperature and solvents removed under reduced pressure. The crude reaction mixture was purified using silica gel column chromatography, 100% ethyl acetate, to produce **2** as a pale yellow solid (1.1 g, 3.3 mmol, 94%) ^{1}H NMR (300 MHz, CDCl$_3$) δ 10.04 (s, 1H), 7.90 (d, J = 8.5 Hz, 2H), 7.77 (d, J = 9.0 Hz, 2H), 7.70 (d, J = 8.5 Hz, 2H), 7.63 (d, J = 9.1 Hz, 2H). ^{13}C{^{1}H} NMR (176 MHz, CDCl$_3$) δ 191.46, 136.09, 132.49, 132.02, 129.78, 128.64, 126.37, 126.34, 126.32, 91.31, 91.07. ^{19}F NMR (282 MHz, CDCl$_3$) δ 83.67 (quintet), 62.84 (d).

Preparation of BD2

Dry DCM (100 mL) containing **2** (1.0 g, 3.0 mmol), 2-methyl-1*H*-pyrrole (0.57 mL, 6.62 mmol) and three drops of trifluoroacetic acid were added to a 250 mL Schlenk tube under an inert nitrogen atmosphere. The resulting reaction mixture was stirred at room temperature for 3 hours. *p*-Chloranil (888 mg, 3.61 mmol) was added portion wise over 10 minutes, and the reaction mixture was stirred at room temperature for 3 hours under an inert nitrogen atmosphere. Diisopropylethylamine (3.7 mL, 21 mmol) was added and stirred at room temperature for 15 minutes. Boron trifluoride diethyl etherate (4.0 mL, 33 mmol) was added and the reaction mixture was stirred at room temperature overnight (∼16 h). The reaction mixture was washed with water (5 × 500 mL). The organic layer was separated, dried over Na$_2$SO$_4$ and the solvent was removed under reduced pressure. Following silica gel column chromatography

(DCM: petroleum ether 40–60 °C, 2 : 3) the product was obtained as a red solid (0.90 g, 1.8 mmol, 60%). ^{1}H NMR (300 MHz, CDCl$_3$) δ 7.77 (d, J = 8.9 Hz, 2H), 7.69–7.59 (m, 4H), 7.51 (d, J = 8.5 Hz, 2H), 6.71 (d, J = 4.1 Hz, 2H), 6.29 (d, J = 4.1 Hz, 2H), 2.66 (s, 6H). ^{13}C{^{1}H} NMR (176 MHz, CDCl$_3$) δ 158.20, 141.42, 134.79, 134.39, 131.94, 131.69, 130.64, 130.29, 126.72, 126.31, 124.34, 120.20, 119.82, 91.51, 89.42, 15.10. ^{11}B NMR (96 MHz, CDCl$_3$) δ 0.95 (t, J = 30.7 Hz). ^{19}F NMR (282 MHz, CDCl$_3$) δ 83.92 (quintet), 62.68 (d, J = 149.9 Hz), −147.53 (q).

Preparation of BD3

Dry DCM (100 mL) containing allyl 4-formylbenzoate **3** (1.0 g, 5.26 mmol), 2,4-dimethyl-1*H*-pyrrole (0.92 mL, 11.57 mmol), and three drops of trifluoroacetic acid were added to a 250 mL Schlenk tube under an inert nitrogen atmosphere. The resulting reaction mixture was stirred at room temperature for 3 hours. DDQ (1.43 g, 6.31 mmol) was added portion wise over 10 minutes, and the reaction mixture was stirred at room temperature for 3 hours under an inert nitrogen atmosphere. Diisopropylethylamine (6.41 mL, 36.8 mmol) was added and stirred at room temperature for 15 minutes. Boron trifluoride diethyl etherate (7.14 mL, 36.8 mmol) was added and the reaction mixture was stirred at room temperature overnight (∼16 h). The reaction mixture washed with water (5 × 500 mL). The organic layer was separated, dried over Na$_2$SO$_4$ and the solvent was removed under reduced pressure. Following silica gel column chromatography (DCM: petroleum ether 40–60 °C, 2 : 3) the product was obtained as a red solid (1.25 g, 3.1 mmol, 58%) ^{1}H NMR (300 MHz, CDCl$_3$) δ 8.20 (d, J = 8.3 Hz, 2H), 7.41 (d, J = 8.3 Hz, 2H), 6.08 (ddt, J = 17.2, 10.4, 5.8 Hz, 1H), 5.99 (s, 2H), 5.46 (dd, J = 17.2, 1.5 Hz, 1H), 5.33 (dd, J = 10.4, 1.3 Hz, 1H), 4.87 (d, J = 5.8 Hz, 2H), 2.55 (s, 6H), 1.36 (s, 6H). ^{13}C{^{1}H} NMR (75 MHz, CDCl$_3$) δ 165.78, 156.15, 143.02, 140.34, 140.08, 132.10, 131.07, 130.95, 130.56, 128.55, 121.63, 118.96, 66.15, 14.67. ^{11}B NMR (96 MHz, CDCl$_3$) δ 0.74 (t, J = 32.3 Hz). ^{19}F NMR (282 MHz, CDCl$_3$) δ −146.23 (quartet, J = 65.5, 32.6 Hz). Mass calc. for C$_{23}$H$_{24}$BF$_2$N$_2$O$_2$ 409.1899 fnd. m/z = 409.1888 [M + H]$^+$.

Preparation of BD5

BD2 (50 mg, 0.096 mmol), *tert*-butyl 4-formylbenzoate **4** (79 mg, 0.38 mmol), and 3 Å molecular sieves (1 g) were added to a 100 mL flame dried Schlenk flask under nitrogen. Dry acetonitrile (20 mL) was added. Piperidine (0.19 mL, 1.91 mmol) was added dropwise followed by glacial acetic acid (0.11 mL, 1.91 mmol). The reaction was stirred at 60 °C for 16 hours. The reaction was cooled, filtered and the solvent was removed under reduced pressure. Following silica gel column chromatography (DCM: petroleum ether 40–60 °C, 3 : 2) the product was isolated as a blue/green solid (10 mg, 0.02 mmol, 19%). ^{1}H NMR (700 MHz, CDCl$_3$) δ 8.04 (d, J = 8.2 Hz, 4H), 7.86 (d, J = 16.3 Hz, 2H), 7.78 (d, J = 8.7 Hz, 2H), 7.73–7.66 (m, 6H), 7.65 (d, J = 8.3 Hz, 2H), 7.56 (d, J = 8.2 Hz, 2H), 7.37 (d, J = 16.3 Hz, 2H), 6.99 (d, J = 4.5 Hz, 2H), 6.84 (d, J = 4.4 Hz, 2H), 1.63 (s, 18H). ^{13}C{^{1}H} NMR (176 MHz, CDCl$_3$) δ 165.48, 154.88, 153.49, 140.23, 139.05, 136.43, 136.12, 134.84, 132.37, 131.96, 131.88, 130.74, 130.12, 129.83, 127.46, 126.69, 126.32, 124.45, 121.24,

117.15, 91.50, 89.62, 81.37, 28.37. ^{19}F NMR (282 MHz, CDCl$_3$) δ 87.39–80.28 (m), 62.67 (d, J = 149.8 Hz), −125.76 to −145.51 (m). ^{11}B NMR (96 MHz, CDCl$_3$) δ 1.30 (t).

Preparation of BD6

Compound **2** (200 mg, 0.49 mmol) and **BD3** (208 mg, 1.96 mmol) were added to a 100 mL 3-necked round bottomed flask. Dry toluene (50 mL) was added followed by piperidine (0.97 mL, 9.80 mmol) and *p*-toluenesulfonic acid (1.69 g, 9.80 mmol). The flask was fitted to a Dean-Stark distillation apparatus. The flask was heated to 150 °C and the water was gradually removed over time. Finally, all the toluene was distilled off and the flask was cooled to room temperature and more dry toluene (50 mL) was added. The flask was heated to 150 °C and the toluene was removed for a second time. The crude reaction mixture was purified using silica gel column chromatography (dichloromethane: petroleum ether 40–60 °C, 3 : 1). The product was isolated as a blue solid (30 mg, 0.029 mmol, 6%). ^{1}H NMR (700 MHz, CDCl$_3$) δ 8.24 (d, J = 8.3 Hz, 2H), 7.87–7.71 (m, 6H), 7.67–7.61 (m, 8H), 7.58 (d, J = 8.3 Hz, 4H), 7.48 (d, J = 8.2 Hz, 2H), 7.26 (d, J = 16.2 Hz, 2H), 6.68 (s, 2H), 6.25–5.99 (m, 1H), 5.64–5.23 (m, 2H), 4.89 (dd, J = 5.9, 1.5 Hz, 2H), 1.45 (s, 6H). ^{13}C{^{1}H} NMR (176 MHz, CDCl$_3$) δ 165.77, 153.24, 152.84, 142.33, 139.99, 137.95, 137.19, 135.74, 133.45, 132.37, 132.09, 131.83, 131.15, 130.61, 128.95, 127.74, 127.08, 126.37–125.99 (m), 122.85, 120.34, 119.03, 118.55, 92.68, 89.32, 66.22. ^{11}B NMR (96 MHz, CDCl$_3$) δ 1.13 (t, J = 33 Hz). ^{19}F NMR (659 MHz, CDCl$_3$) δ −137.81 (quartet, J = 66 Hz, 33 Hz), −73.20 (s), −72.11 (s). Mass calc. for C$_{53}$H$_{37}$BF$_{12}$N$_2$O$_2$S 1036.2198 fnd. m/z = 1036.6705 [M]$^{+}$.

X-Ray diffraction

All crystal structure data were collected at 150 K using copper radiation ($\lambda_{CuK\alpha}$ = 1.54184 Å) on an Xcalibur, Atlas, Gemini ultra diffractometer equipped with an Oxford Cryosystems Cryo-streamPlus open-flow N$_2$ cooling device. The intensities were corrected for absorption empirically using a multifaceted crystal model created by indexing the faces of the crystal for which data were collected.[20] Cell refinement, data collection and data reduction were undertaken *via* the software CrysAlisPro.[21]

All structures were solved using XT[22] and refined by XL[23] using the Olex2 interface.[24] All non-hydrogen atoms were refined anisotropically and hydrogen atoms were positioned with idealised geometry, with the exception of those bound to heteroatoms where the positions could be located using peaks in the Fourier difference map. The displacement parameters of the hydrogen atoms were constrained using a riding model with $U_{(H)}$ set to be an appropriate multiple of the U_{eq} value of the parent atom.

Author contributions

RDJ carried out all the synthetic work, characterization and spectroscopic work with supervision from FC and ACB. All crystallographic work was performed by PGW. Manuscript preparation was carried out by ACB with contributions from all the other authors.

Conflicts of interest

There are no conflicts to declare.

Notes and references

1 (*a*) N. Boens, V. Leen and W. Dehaen, *Chem. Soc. Rev.*, 2012, **41**, 1130–1172; (*b*) T. Zhang, C. Ma, T. Sun and Z. Xie, *Coord. Chem. Rev.*, 2019, **390**, 76–85; (*c*) W. Zhang, A. Ahmed, H. Cong, S. Wang, Y. Shen and B. Yu, *Dyes Pigm.*, 2021, **185**, 108937; (*d*) F.-Z. Li, J.-F. Yin and G.-C. Kuang, *Coord. Chem. Rev.*, 2021, **448**, 214157; (*e*) A. Barattucci, C. M. A. Gangemi, A. Santoro, S. Campagna, F. Puntoriero and P. Bonaccorsi, *Org. Biomol. Chem.*, 2022, **20**, 2742–2763; (*f*) N. Boens, B. Verbelen, M. J. Ortiz, L. Jiao and W. Dehaen, *Coord. Chem. Rev.*, 2019, **399**, 213024; (*g*) H. Lu, J. Mack, Y. Yang and Z. Shen, *Chem. Soc. Rev.*, 2014, **43**, 4778–4823.

2 (*a*) A. Loudet and K. Burgess, *Chem. Rev.*, 2007, **107**, 4891–4932; (*b*) M. Liu, S. Ma, M. She, J. Chen, Z. Wang and P. Lui, *Chin. Chem. Lett.*, 2019, **30**, 1815–1824; (*c*) Y. Qin, X. Lui, P.-P. Jia and H.-B. Yang, *Chem. Soc. Rev.*, 2020, **49**, 5678–5703; (*d*) E. Bodio and C. Goze, *Dyes Pigm.*, 2019, **160**, 700–710; (*e*) A. Kamkaew, S. H. Lim, H. B. Lee, L. V. Kiew, L. Y. Chung and K. Burgess, *Chem. Soc. Rev.*, 2013, **42**, 77–88; (*f*) L. Jean-Gerard, W. Vasseur, F. Scherninski and B. Andrioletti, *Chem. Commun.*, 2018, **54**, 12914–12929.

3 (*a*) R. Ziessel, G. Ulrich and A. Harriman, *New J. Chem.*, 2007, **31**, 496–501; (*b*) N. A. Bumagina, E. V. Antina, A. A. Ksenofontov, L. A. Antina, A. A. Kalyagin and M. B. Berezin, *Coord. Chem. Rev.*, 2022, **469**, 214684; (*c*) G. Ulrich, R. Ziessel and A. Harriman, *Angew. Chem., Int. Ed.*, 2008, **47**, 1184–1201.

4 M. A. H. Alamiry, A. C. Benniston, J. Hagon, T. P. L. Winstanley, H. Lemmetyinen and N. V. Tkachenko, *RSC Adv.*, 2012, **2**, 4944–4950.

5 P. Gautam, C. P. Yu, G. Zhang, V. E. Hillier and J. M. W. Chan, *J. Org. Chem.*, 2017, **82**, 11008–11020; X. Niu, P. Gautam, Z. Kuang, C. P. Yu, Y. Guo, H. Song, Q. Guo, J. M. W. Chan and A. Xia, *Phys. Chem. Chem. Phys.*, 2019, **21**, 17323–17331.

6 D. Kerwat, S. Grätz, J. Kretz, M. Seidel, M. Kunert, J. B. Weston and R. D. Süssmuth, *ChemMedChem*, 2016, **11**, 1899–1903.

7 L. S. Alqahtani, R. D. James, J. Mallows, H. V. Flint, P. G. Waddell, O. Woodford and E. A. Gibson, *Sustainable Energy Fuels*, 2023, **7**, 1494–1501.

8 B. Herrado, A. Chana, M. Alonso, F. Amat-Guerria, M. Liras and M. A. Maestro, *J. Mol. Struct.*, 2004, **697**, 29–40.

9 P. Geerlings, F. De Proft and W. Langenaeker, *Chem. Rev.*, 2003, **103**, 1793–1873.

10 W. Qin, M. Baruah, M. Van der Auweraer, F. C. De Schryver and N. Boens, *J. Phys. Chem. A*, 2005, **109**, 7371–7384.

11 D. H. McDaniel and H. C. Brown, *J. Org. Chem.*, 1958, **23**, 420–427.

12 W. A. Sheppard, *J. Am. Chem. Soc.*, 1962, **84**, 3072–3076.

13 P. Gautam, Y. Wang, G. Zhang, H. Sun and J. M. W. Chan, *Chem. Mater.*, 2018, **30**, 7055–7066.

14 O. Exner and S. Böhm, *New J. Chem.*, 2008, **32**, 1449–1453.

15 (*a*) E. Z. Lippert, *Z. Naturforsch., A: Astrophys., Phys. Phys. Chem.*, 1955, **10a**, 541–545; (*b*) N. Mataga, Y. Kaifu and M. Koizumi, *Bull. Chem. Soc. Jpn.*, 1956, **29**, 465–470.

16 S. G. Telfer, T. M. McLean and M. R. Waterland, *Dalton Trans.*, 2011, **40**, 3097–3108.

17 M. Kasha, H. R. Rawls and M. A. El-Bayoumi, *Pure Appl. Chem.*, 1965, **11**, 371–392.

18 A. M. Brouwer, *Pure Appl. Chem.*, 2011, **83**, 2213–2228.

19 M. J. Frisch, G. W. Trucks, H. B. Schlegel, G. E. Scuseria, M. A. Robb, J. R. Cheeseman, G. Scalmani, V. Barone, G. A. Petersson, H. Nakatsuji, X. Li, M. Caricato, A. Marenich, J. Bloino, B. G. Janesko, R. Gomperts, B. Mennucci, H. P. Hratchian, J. V. Ortiz, A. F. Izmaylov, J. L. Sonnenberg, D. Williams-Young, F. Ding, F. Lipparini, F. Egidi, J. Goings, B. Peng, A. Petrone, T. Henderson, D. Ranasinghe, V. G. Zakrzewski, J. Gao, N. Rega, G. Zheng, W. Liang, M. Hada, M. Ehara, K. Toyota, R. Fukuda, J. Hasegawa, M. Ishida, T. Nakajima, Y. Honda, O. Kitao, H. Nakai, T. Vreven, K. Throssell, J. A. Montgomery Jr., J. E. Peralta, F. Ogliaro, M. Bearpark, J. J. Heyd, E. Brothers, K. N. Kudin, V. N. Staroverov, T. Keith, R. Kobayashi, J. Normand, K. Raghavachari, A. Rendell, J. C. Burant, S. S. Iyengar, J. Tomasi, M. Cossi, J. M. Millam, M. Klene, C. Adamo, R. Cammi, J. W. Ochterski, R. L. Martin, K. Morokuma, O. Farkas, J. B. Foresman and D. J. Fox, *Gaussian 09, Revision A.02*, Gaussian, Inc., Wallingford CT, 2016.

20 R. C. Clark and J. S. Reid, *Acta Crystallogr., Sect. A: Found. Crystallogr.*, 1995, **51**, 887–897.

21 *CrysAlisPro*, Rigaku Oxford Diffraction, Tokyo, Japan.

22 G. M. Sheldrick, *Acta Crystallogr., Sect. A: Found. Crystallogr.*, 2015, **71**, 3–8.

23 G. M. Sheldrick, *Acta Crystallogr., Sect. A: Found. Crystallogr.*, 2008, **64**, 112–122.

24 O. V. Dolomanov, L. J. Bourhis, R. J. Gildea, J. A. K. Howard and H. J. Puschmann, *Appl. Crystallogr.*, 2009, **42**, 339–341.